Remote Sensing of Environment 183 (2016) 294–303

Contents lists available at ScienceDirect

Remote Sensing of Environment

journal homepage: www.elsevier.com/locate/rse

Derivation and validation of supraglacial lake volumes on the Greenland Ice Sheet from high-resolution satellite imagery

Mahsa S. Moussavi [a,b,c,*], Waleed Abdalati [a], Allen Pope [a,c], Ted Scambos [a,c], Marco Tedesco [d,e], Michael MacFerrin [a,b], Shane Grigsby [a,b]

[a] Cooperative Institute for Research in Environmental Sciences (CIRES), University of Colorado Boulder, USA
[b] Earth Science and Observation Center (ESOC), University of Colorado Boulder, USA
[c] National Snow and Ice Data Center (NSIDC), University of Colorado Boulder, USA
[d] Lamont-Doherty Earth Observatory of Columbia University, Palisades, NY, USA
[e] NASA Goddard Institute of Space Studies, NY, USA

ARTICLE INFO

Article history:
Received 1 September 2015
Received in revised form 16 May 2016
Accepted 28 May 2016
Available online xxxx

Keywords:
Greenland Ice Sheet hydrology
Supraglacial water depth
Spectrally-based depth-retrieval models
WorldView-2 satellite
High-resolution digital elevation model (DEM)

ABSTRACT

Supraglacial meltwater lakes on the western Greenland Ice Sheet (GrIS) are critical components of its surface hydrology and surface mass balance, and they also affect its ice dynamics. Estimates of lake volume, however, are limited by the availability of in situ measurements of water depth, which in turn also limits the assessment of remotely sensed lake depths. Given the logistical difficulty of collecting physical bathymetric measurements, methods relying upon in situ data are generally restricted to small areas and thus their application to large-scale studies is difficult to validate. Here, we produce and validate spaceborne estimates of supraglacial lake volumes across a relatively large area (1250 km^2) of west Greenland's ablation region using data acquired by the WorldView-2 (WV-2) sensor, making use of both its stereo-imaging capability and its meter-scale resolution. We employ spectrally-derived depth retrieval models, which are either based on absolute reflectance (single-channel model) or a ratio of spectral reflectances in two bands (dual-channel model). These models are calibrated by using WV-2 multispectral imagery acquired early in the melt season and depth measurements from a high resolution WV-2 DEM over the same lake basins when devoid of water. The calibrated models are then validated with different lakes in the area, for which we determined depths. Lake depth estimates based on measurements recorded in WV-2's blue (450–510 nm), green (510–580 nm), and red (630–690 nm) bands and dual-channel modes (blue/green, blue/red, and green/red band combinations) had near-zero bias, an average root-mean-squared deviation of 0.4 m (relative to post-drainage DEMs), and an average volumetric error of <1%. The approach outlined in this study – image-based calibration of depth-retrieval models – significantly improves spaceborne supraglacial bathymetry retrievals, which are completely independent from in situ measurements.

1. Introduction

The acceleration of mass loss from the Greenland Ice Sheet (GrIS) over the last two decades is of great significance when considering its potential contribution to sea level rise (Wouters, Chambers, & Schrama, 2008; van den Broeke et al., 2009; Schrama & Wouters, 2011; Rignot, Velicogna, van den Broeke, Monaghan, & Lenaerts, 2011; Shepherd et al., 2012). Accurate projections of Greenland's contribution to sea level rise require an improved understanding of ice dynamic responses to hydrologic processes, which is currently lacking (Bartholomew et al., 2012; Bartholomew et al., 2011; Das et al., 2008; Hoffman, Catania, Neumann, Andrews, & Rumrill, 2011; Palmer, Shepherd, Nienow, & Joughin, 2011; Zwally et al., 2002; Phillips, Rajaram, Colgan, Steffen, & Abdalati, 2013; Tedesco et al. 2013a). Supraglacial lakes and streams play a crucial role in the ice sheet's hydrological system by storing large quantities of meltwater, which can promote hydrofracturing events (i.e. propagation of water-filled cracks to the base of the ice sheet). A sudden influx of meltwater to the ice-bed interface, as a result of hydrofracturing events, can increase basal water pressures and therefore overwhelm existing drainage systems, leading to pronounced yet short-lived enhancements of ice flow (Das et al., 2008; Catania, Neumann, & Price, 2008; Hoffman et al., 2011; Selmes, Murray, & James, 2011; Selmes, Murray, & James, 2013). This process, however, is largely controlled by the rate of meltwater delivery to the subglacial environment. Slow vs. rapid drainage events appear to impact ice dynamics differently (Tedesco et al., 2013b; Stevens et al., 2015). Thus, to advance the coupling between hydrological and ice dynamics models, it is important to quantify how much meltwater is stored on the ice sheet in supraglacial lakes and ponds, how much

* Corresponding author at: Cooperative Institute for Research in Environmental Sciences (CIRES), University of Colorado Boulder, USA.

http://dx.doi.org/10.1016/j.rse.2016.05.024
0034-4257/

drains from the ice sheet surface through supraglacial streams and rivers, and how much drains into the ice sheet through crevasses and moulins (Smith et al., 2015). Making assessments of water volumes, however, is quite challenging, as it requires knowledge of bathymetry over supraglacial water bodies, which is very difficult to measure especially over large areas. Given the distribution of supraglacial lakes across large areas of the ice sheet, data from spaceborne optical sensors offer great potential for this purpose.

The fundamental concept behind spaceborne bathymetry is to build depth-reflectance relationships in order to isolate the effects of depth, water column optical properties, and bottom albedo on measured reflectance. Several physically-based and empirical passive remote sensing techniques have been used to derive bathymetric information over supraglacial lakes using the Moderate Resolution Imaging Spectroradiometer (MODIS), the Advanced Spaceborne Thermal Emission and reflection Radiometer (ASTER), Landsat 7, Landsat 8, or WorldView-2 (WV-2) measurements (Sneed & Hamilton, 2007; McMillan, Nienow, Shepherd, Benham & Sole, 2007a; Box & Ski, 2007; Georgiou, Shepherd, McMillan & Nienow, 2009; Tedesco & Steiner, 2011a, 2011b; Legleiter, Tedesco, Smith, Behar & Overstreet, 2014; Banwell et al., 2014; Pope et al., 2016). Though providing valuable insight into supraglacial bathymetry, previous efforts have been hindered by the paucity of co-located remote sensing and in situ observations of water depth and spectral reflectance. Most of the techniques reported in the literature rely solely upon sparse point measurements to calibrate reflectance to depth, or to validate estimated water depths (e.g. Tedesco & Steiner, 2011a, 2011b; Legleiter et al., 2014). Therefore these studies were confined to small areas and to a limited number of lakes out of necessity. Furthermore, some of these techniques have been applied across large portions of the ablation region, despite not being validated at large spatial scales (e.g. Fitzpatrick et al., 2014; Arnold, Banwell & Willis, 2014).

The main goal of our study is to explore the capability of the WV-2 sensor in retrieving validated supraglacial lake depths over large areas that are independent from in situ measurements. Although this study primarily focuses on the use of WV-2 measurements, we also estimate lake depths from data collected by Landsat 7's Enhanced Thematic Mapper (ETM$^+$). Given the vast archive of Landsat 7 imagery, developing models for the ETM$^+$ sensor will be useful for expanding lake volumes assessments, which are required for large-scale studies of ice sheet surface hydrology.

2. Study area and data description

The primary study area (50 km × 25 km) is located in the ablation region of the GrIS, centered at 67° 16′ 33″ N, 49° 35′ 15″ W and approximately 1200 m above sea level (a.s.l) (Fig. 1), over which imagery from WV-2 and Landsat 7 ETM$^+$ sensors was available. We used two WV-2 multispectral images (~2 m resolution) covering the area from early in the melt season (June 12, 2011) and six stereo panchromatic WV-2 pairs (~0.5 m resolution) over the same area at the end of the melt season (August 30, 2011). WV-2 instrument acquires data in eight spectral bands, namely coastal blue (400–450 nm), blue (450–510 nm), green (510–580 nm), yellow (585–625 nm), red (630–690 nm), red edge (705–745 nm), Near InfradRed-1 (770–895 nm), and Near InfraRed-2 (860–1040 nm). However, the multispectral WV-2 images over our study area were acquired with just four of the 8 available spectral bands, notably blue, green, red, and Near InfraRed-1.

The Landsat 7 image over the study site was acquired on the same day as the WV-2 scenes (within ~1 h). Of the total twenty-two lakes visible in Fig. 1, we used measurements over fourteen large lakes for which we were able to acquire stereo image pairs following their drainage later in the season.

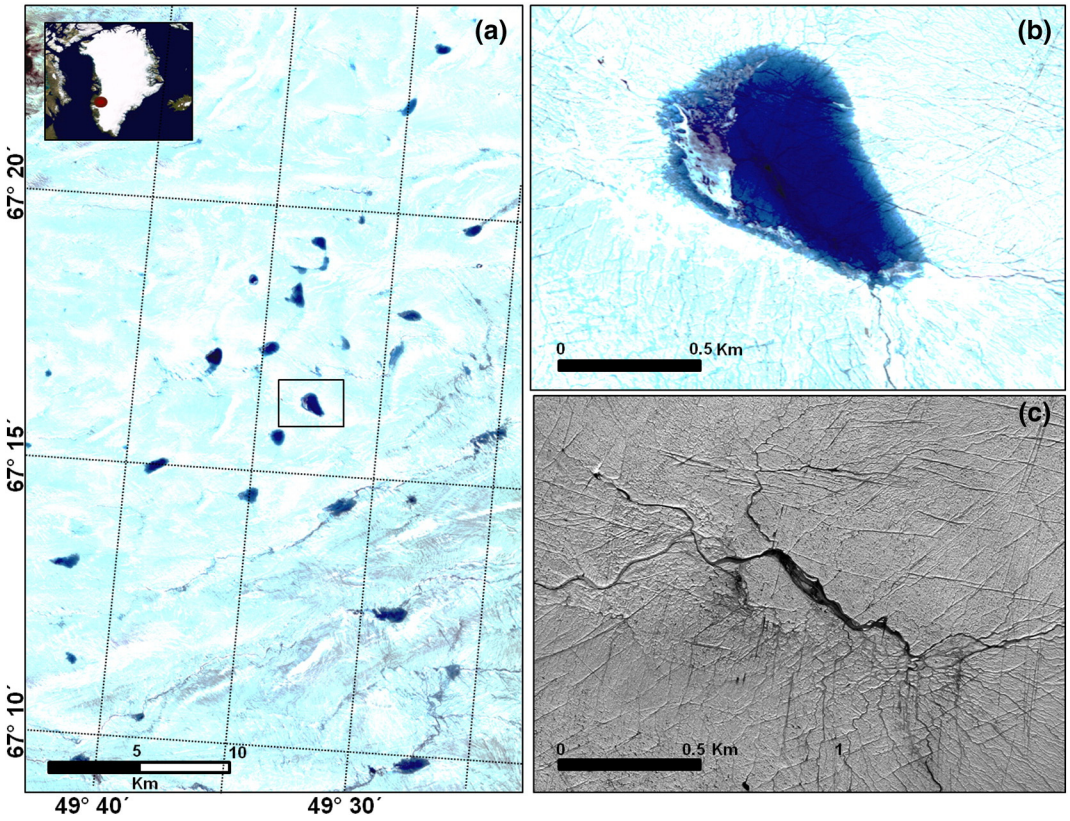

Fig. 1. (a) Enhanced true-color composite mosaic of WV-2 images acquired over the primary study area. Visible in the composite are twenty-two large lakes with an average areal extent of 1.5 km^2. (b) The enlarged boxes show WV-2 snapshots of a lake pre-drainage on June 12, 2011 and (c) post-drainage on August 30, 2011 included in the black box shown in the left panel. (For interpretation of the references to color in this figure legend, the reader is referred to the web version of this article.)

The second study site is a lake (0.85 km across) located at 69° 36′ 42″ N and 49° 30′ 10″S in west Greenland (Fig. 2), over which concurrent in situ measurements of depth (ranging from 1 to 4.6 m) and spectral reflectance (450–1050 nm) were available (1 m spatial resolution, 0.3 nm spectral resolution) (Tedesco & Steiner, 2011a, 2011b). Data (n = 2226) were collected by a remotely-controlled boat, which was equipped with a GPS/sonar, an above-surface irradiance sensor, a below-surface downward looking radiance sensor, a spectrometer, and a microcomputer. The uncertainty in depth measurements was estimated to be on the order of 0.2–0.3 m (Tedesco & Steiner, 2011a, 2011b). We used in situ measurement over this second study site to further assess the capability of WV-2 spectral bands in retrieving supraglacial lake depths.

3. Methodology

We calibrated single- and dual-channel bathymetric models by utilizing water reflectance over supraglacial lakes captured by the WV-2 and Landsat 7 ETM$^+$ sensors early in the melt season and depth measurements derived from a high resolution WV-2 DEM over the same lake basins when drained at the end of the melt season. The following provides a detailed description of the methodology used in this study.

3.1. Image pre-processing

Bathymetric modeling from satellite imagery requires an accurate surface reflectance retrieval, necessitating both geometric and radiometric correction of the satellite scenes. Geometrically-corrected WV-2 images, have a geolocation accuracy of better than 3.5 m horizontal 90% circular error of probability (DigitalGlobe, 2014). For atmospheric correction, we used the MODerate resolution Transmission (MODTRAN5) radiative transfer code to model transmittance and remove path radiance (Berke, 2006). The MODTRAN inputs of total column ozone (308.2 Dobson units) and water vapor (0.74 g cm^{-2}) were derived from the MODIS MOD07 atmospheric product (Menzel et al., 2002). The MODIS overpass selected was within one hour of the WV-2 scene acquisition, had viewing zenith angles <30°, and did not have any aberrant Quality Assurance and Quality Control flags. Additional MODTRAN inputs such as acquisition time, location, and viewing geometry were set to match those of the WV-2 and Landsat 7 sensors at image acquisition. The MODTRAN output was convolved (Schläpfer & Nieke, 2005) using the spectral response functions of WV-2 (Padwick, 2010) and Landsat (Flood, 2014). The convolved output for path radiance and transmittance was used to atmospherically correct the sensor observed radiance to surface-leaving radiance, ultimately yielding surface reflectance suitable for bathymetric modeling.

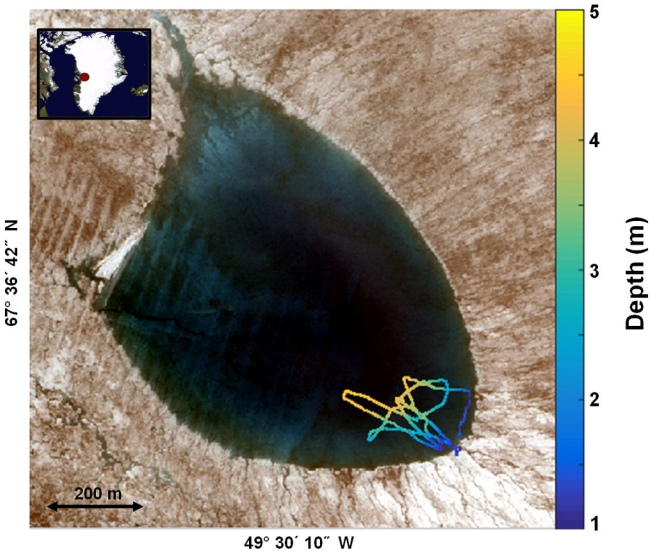

Fig. 2. True color composite of a WV-2 scene showing the second study area, situated at 69° 36′ 42″ N and 49° 30′ 10″ S. Contemporaneous in-situ measurements of spectral reflectance and depth were collected by a remotely controlled boat (Tedesco & Steiner, 2011a, 2011b), which was deployed on 2, 3, and 5 July 2010.

Table 1
Parameters for and statistics on lake depth retrieval using a physically-based single-channel technique (Eq. (2)). Calibration datasets based on WV-2 and ETM$^+$ imagery consisted of $n_{WV\text{-}2} = 430{,}899$ and $n_{L7} = 4689$ depth-reflectance pairs, respectively.

Central wavelength λ_c (nm)	Lake bed albedo (A_d)	Attenuation coefficient (g) (m^{-1})	Reflectance of optically-deep water (R_∞)	R^2	Std. dev. (m)
WorldView-2 calibration dataset					
Blue: 480	0.59	0.16	0.14	0.72	0.59
Green: 545	0.52	0.28	0.12	0.77	0.48
Red: 660	0.28	0.73	0.03	0.71	0.49
Landsat 7 ETM$^+$ calibration dataset					
Blue: 485	0.48	0.16	0.07	0.81	0.57
Green: 560	0.40	0.29	0.05	0.81	0.53
Red: 660	0.19	0.69	0.03	0.70	0.76

3.2. Delineation of supraglacial lakes in WorldView-2 and Landsat 7 imagery

To isolate supraglacial lake pixels in WV-2 scenes, we used the enhanced Normalized Difference Water Index ($NDWI_{enhanced}$) method developed by Yang and Smith (2013). Given the relatively strong contrast between water and ice in the red band (630–690 nm), and the high spectral reflectance of water in the blue band (450–510 nm), NDWI classifies the image into "water" and "non-water" regions using a threshold based on Eq. (1).

$$NDWI_{enhanced} = \frac{Blue - Red}{Blue + Red} \quad (1)$$

The choice of threshold can be adjusted to identify lakes, streams or slush. In this study, we only used reflectances recorded over lakes to calibrate models since lakes span a broader range of depths as compared to streams and rivers. To calculate a threshold suitable for water detection, we averaged $NDWI_{enhanced}$ values over thousands of randomly selected lake pixels of variable depths. The selected threshold (0.23) was suitable for extracting lake pixels; however, some supraglacial stream pixels were misclassified as lakes. To better delineate only lake boundaries, we used the opening morphological operator. This process first erodes the classified features in a binary mask and then dilates them according to the structuring element (kernel). Small narrow features, such as streams, were removed from the results, while the large lakes remained intact. We followed a similar approach to identify lake pixels in the Landsat 7 scene of our study site.

3.3. Digital depth model (DDM) generation from WV-2 stereo imagery

We created a Digital Elevation Model (DEM) from overlapping pairs of high-resolution (50 cm) WV-2 panchromatic stereo images acquired over our study area (Fig. 1), which represented surface topography at the end of the 2011 melt season. The DEM, gridded at 4 m resolution, was constructed based on satellite positioning parameters (Rational

Table 2
Parameters for and statistics on lake depth retrieval using an empirical single-channel technique (Eq. (3)) and WV-2 calibration dataset (n = 430,899).

λ_c (nm)	($\propto_0$)	($\propto_1$)	($\propto_2$)	R^2	Std. dev. (m)
Blue: 480	−7.48	0.16	9.82	0.72	0.61
Green: 545	−2.96	0.08	4.88	0.76	0.52
Red: 660	−0.42	0.03	1.34	0.70	0.48

Table 3
Sensitivity of derived depth to a 1% change in single-channel model (Eq. (2)) parameters for WV-2's blue, green, and red spectral channels. These values are averaged over a possible range of water reflectances in each spectral channel.

λ (nm)	Error (m) (1%ΔA_d)	Error (m) (1%Δg)	Error (m) (1%ΔR_∞)
Blue (480)	0.08	0.09	0.02
Green (545)	0.05	0.05	0.01
Red (660)	0.02	0.01	0.00

Polynomial Coefficients) using the Leica Photogrammetry Suite Module of ERDAS® IMAGINE software. The absolute vertical accuracy of the derived DEM products is <5.0 m with submeter relative vertical precision, which is estimated to be within 0.15–0.3 m (Mitchell, 2010; Aguilar, del Mar Saldana, & Aguilar, 2014; Willis, Herried, Bevis, & Bell, 2015; Shean et al., 2016). Based on lake boundaries (see Section 3.1), we averaged the DEM-derived surface elevations over lake shoreline pixels and subtracted the shoreline elevation from lake floor elevations to produce Digital Depth Models (DDMs) for individual lakes. We found the elevations of lake shoreline pixels to be constant within ±0.30 m, which combines DEM vertical precision and the horizontal uncertainty of lake boundaries. Using the resulting DDMs and lake spectral reflectances collected by the WV-2 sensor (see Section 4.), we produced a depth-reflectance dataset consisting of $n_{WV\text{-}2} = 710{,}253$ measurement pairs (i.e. measurements of both lake depth and reflectance). To build a depth-reflectance dataset based on Landsat 7 ETM$^+$ imagery, we resampled the DDMs to 30 m resolution using bi-linear interpolation, resulting in 7676 depth-reflectance measurement pairs over our primary study site.

3.4. Spectrally-based depth-retrieval

To establish depth-reflectance relationships, we employed three spectrally-based models that are widely used in the literature. These included physically-based (Philpot, 1989; Sneed & Hamilton, 2007), empirical single-channel models (Box & Ski, 2007), and an empirical dual-channel model (Legleiter et al., 2014). The following provides descriptions for each of these bathymetric models, and how we applied them.

3.4.1. Physically-based single-channel model

Irradiance passing through a water column is attenuated exponentially with depth, due to absorption and scattering processes (e.g. Swinehart, 1962). Philpot (1989) derived an expression to determine water depth from passive optical data, which is described as

$$z = g^{-1}[\ln(A_d - R_\infty) - \ln(R_w - R_\infty)] \quad (2)$$

where $A_d$is the bottom or substrate albedo (reflectance), R_∞ is the reflectance for optically deep water (>40 m), R_w is the observed water-leaving reflectance, and z is water depth. The quantity g is a two-way attenuation coefficient that accounts for losses in both upward and downward directions including absorption and scattering. Once the three model parameters (A_d, g, R_∞) have been determined, Eq. (2) provides a means of retrieving depth from measured surface reflectance.

Sneed and Hamilton (2007) proposed an algorithm for finding appropriate values for model parameters based on multispectral ASTER data. While their approach offers valuable insight into space-based bathymetry, it has limited applicability for WV-2 because it requires images covering both ice sheet margin and ice-free ocean (R_∞ is estimated based on the reflectance of deep ocean water far from the coast). Moreover, it relies on several assumptions about the optical properties of water and ice, which may introduce significant errors to depth estimation. Based on depth-reflectance datasets previously developed for the WV-2 and ETM+ sensors (Section 3.3), three model parameters in Eq. (2) (A_d, g, R_∞) were derived by solving a system of nonlinear equations (based on Eq. (2)) through Levenberg-Marquardt least-squared regression (Markwardt, 2009).

3.4.2. Empirical single-channel model

We extended our analysis to calibrate the depth-reflectance function (Eq. 3) proposed by Box and Ski (2007), in which MODIS reflectance and in situ depth measurements of two supraglacial lakes were coupled to develop a depth-retrieval model. They approximated the observed depth-reflectance scatter by a least-square fit of the form:

$$D = \propto_0 (R + \propto_1)^{-1} + \propto_2 \quad (3)$$

where D is the lake depth and R is MODIS band 1 (620–670 nm) reflectance. We derived the three model parameters ($\propto_0$, $\propto_1$, $\propto_2$) through regressions of depth against reflectance according to Eq. (3).

3.4.3. Dual-channel model

The logarithm of the ratio of reflectances recorded in two spectral channels is relatively constant across variable bottom types, as changes in bottom reflectance affect both bands similarly (Legleiter et al., 2009). Under appropriate conditions (as summarized by Legleiter et al. (2009)), the radiometric quantity defined by this ratio ($X = \ln[\frac{R_w(\lambda_1)}{R_w(\lambda_2)}]$, where $R_w(\lambda_i)$ is lake reflectance recorded in a given spectral channel) can be assumed to be quadratically related to depth (D):

$$D = aX^2 + bX + c \quad (4)$$

Following a method proposed by Legleiter et al. (2009), namely Optimal Band Ratio Analysis (OBRA), we found the most appropriate

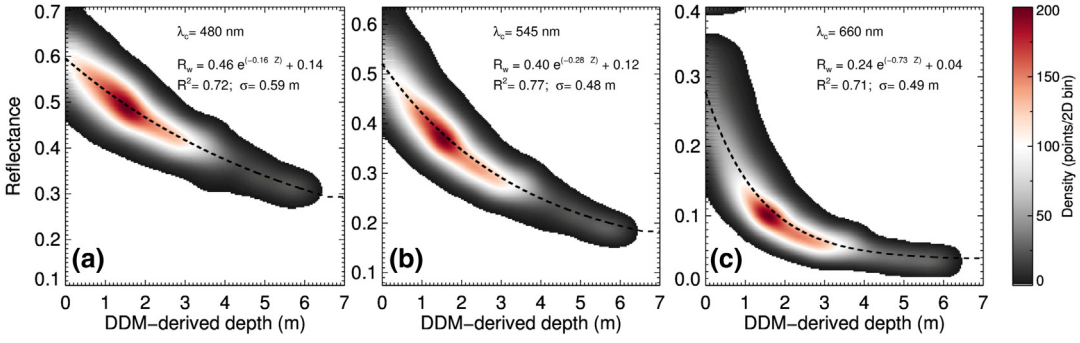

Fig. 3. Density plots of depth-reflectance observations for three WV-2 channels (n = 430,899). The dashed lines represent the best fits for the physically-based single-channel model (Eq. (2)). The density values were defined based on a 2D histogram with a pixel size of 0.035 m by 0.003 in the x (depth) and y (reflectance) directions, respectively. a) Blue channel (λ_c=480 nm), b) green channel (λ_c=545 nm), and c) red channel (λ_c=660 nm). (For interpretation of the references to color in this figure legend, the reader is referred to the web version of this article.)

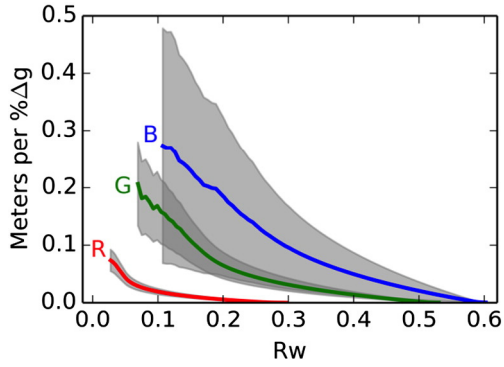

Fig. 4. Changes in depth (z) per 1% change in the parameter g in the single-channel model for WV-2's red, green, and blue channels as a function of water reflectance. Means and standard deviations are shown from the Monte Carlo simulation. (For interpretation of the references to color in this figure legend, the reader is referred to the web version of this article.)

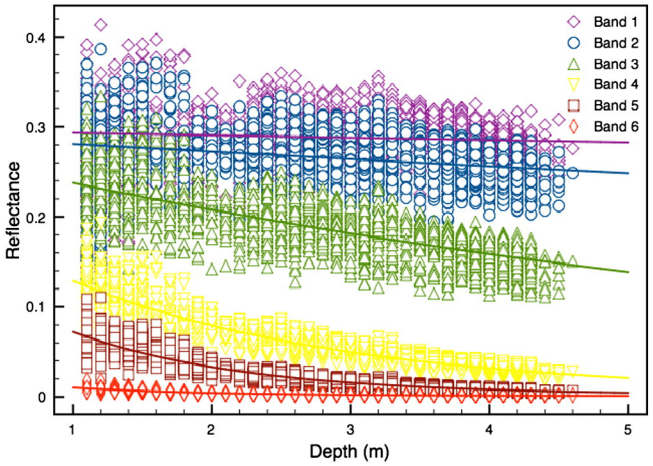

Fig. 6. Simulated WV-2 reflectances (bands 1–6) vs. sonar-derived lake depth. The curves represent the best exponential fits according to the physically-based single-channel model (Eq. (2)).

bathymetric method by finding the pair of wavelengths that yields the highest R^2 among regressions of D on X, according to Eq. (4), for all possible band combinations.

4. Results and discussion

4.1. Calibration of spectrally-based depth retrieval models from satellite image data

Calibration relationships were established based on a random subset of our depth-reflectance dataset (i.e. data from a random group of lakes (seven lakes), which included the deepest lake in the study area), referred to as the calibration dataset hereafter. Calibration datasets based on WV-2 and L7 ETM$^+$ imagery consisted of $n_{WV\text{-}2} = 430{,}899$, and $n_{L7} = 4605$ measurement pairs, respectively. We used the remaining data (i.e. data from seven other lakes not used in the calibration step), referred to as the validation dataset, to independently assess the accuracy of the spectrally-retrieved depths.

4.1.1. Single-channel model calibration

Tables 1 and 2 provide a summary of the retrieved parameters for physically-based and empirical single-channel models along with their corresponding statistics.

The applicability of depth-reflectance relationships is limited by a depth threshold, beyond which the increase in depth no longer reduces spectral reflectance. Since the lake depths in our study area were <7 m we were unable to determine cut-offs for blue and green channels. However, for red channel, the absorption of light at depths >5 m appeared to be too strong to have any further effect on reflectance (Fig. 3). As can be noted from Tables 1 and 2, the physical and empirical models have similar statistical performances in capturing variations of reflectance with depth. Using either technique, however, WV-2's green and red band data would be most suitable for deriving lake depths, in terms of accuracy and sensitivity to water depths. Analysis of the single-channel method based on the ETM$^+$ dataset resulted in similar findings, although we note a discrepancy between retrieved lake bed albedo and optically-deep water reflectances based on WV-2 and L7 images (Table 1). This discrepancy is most likely due to different viewing geometries for the two sensors. The Landsat image was collected from a downward looking geometry, while the WV-2 scene was collected with 15° look zenith and a 45° sun zenith, and azimuths that were complimentary. Therefore, there will be more surface reflectance visible to WV-2 than to Landsat. Similar to WV-2, L7's blue and green bands performed similarly well ($R^2 = 0.81$, see Table 1). Again, as expected, L7's red band, while producing accurate results ($R^2 = 0.70$), showed sensitivity to lake depths up to 5 m.

We compared numerically-derived lake bed albedos (A_d) (Table 1) to those obtained by averaging reflectances over lake shorelines. We found that mean lake margin reflectances were consistently higher than optimized albedos by 5–10%, which directly translates into an average depth underestimation of ~15–25%, across various wavelengths (see Table 3). Therefore, based on our analysis, it does not appear to be appropriate to assume similar reflective properties between central lake substrate and shallow lake edges. Tedesco et al. (2012) speculated that different ablation rates between ice exposed at the bottom of a lake and that around a lake edge could be responsible for their different reflective properties, especially for lakes with longer lifetimes.

We compared optimized attenuation coefficients (g) (Table 1) to theoretical (pure water) values from Pope and Fry (1997) and Smith and Baker (1981) and found that using laboratory values leads to

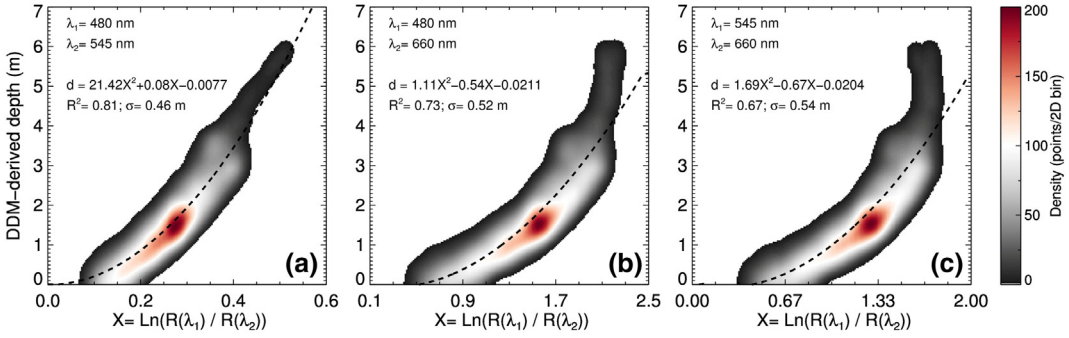

Fig. 5. Density plots of depth (d) versus ($X = \ln\frac{R(\lambda_1)}{R(\lambda_2)}$) relationships based on WV-2 calibration dataset ($n = 430{,}899$) and dual-channel method (Eq. (4)). a) Blue & green ratio transform, b) blue & red ratio transform, and c) green & red ratio transform. (For interpretation of the references to color in this figure legend, the reader is referred to the web version of this article.)

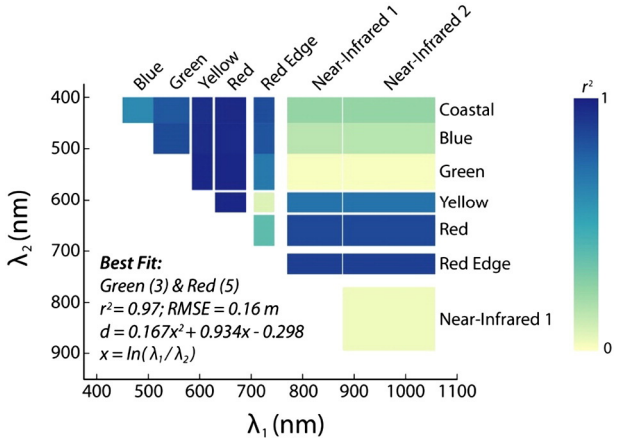

Fig. 7. Success of quadratic optimal band ratio analysis for WV-2 band pairs simulated by in situ spectra (Eq. (4)).

depth overestimation by 80% and 60% in blue and green channels, respectively, and depth underestimation by 6% in the red channel. Such discrepancies between optimized and theoretical values could be indicative of a higher concentration of suspended or dissolved matter in supraglacial water than generally assumed. Therefore, for WV-2 we cannot simply rely on theoretical values of freshwater absorption and scattering to fully represent attenuation conditions in meltwater lakes. However, Pope et al. (2016) were able to successfully retrieve supraglacial lake depths using lab-measured values with Landsat 8 data to an accuracy of 0 ± 1.6 m.

To address the sensitivity of the non-linear single-channel model to uncertainties in each model parameter, we ran Monte-Carlo simulations against each of the model parameters used in the analysis (A_d, g, R_∞), with N = 1000 samples derived from normal distributions of each parameter, providing 10^9 model samples per reflectance value (R_w) for each parameter and each channel. The parameter distributions (mean and standard deviation) are noted in Table 1. Each parameter was isolated independently to assess the sensitivity of the model to small changes in that parameter across a range of reflectances at each wavelength.

Lake depths derived from the single-channel model were least sensitive to uncertainties in model parameters (A_d, g, R_∞) when using the red channel, more sensitive for the green channel, and most sensitive with the blue channel (Table 3), thus making red channel reflectances most suitable for accurate lake depth retrieval. This finding is consistent with the validation results in this paper (see Section 4.3.1). The simulation results indicate consistent model sensitivity to A_d and R_∞ across all reflectance values for a specific channel; however, with respect to uncertainties introduced by the parameter "g", results showed a strong dependence on the magnitude of reflectance (R_w,) as noted in Fig. 4. A 1% uncertainty in "g" causes the largest error in depth at the lowest reflectance values (deeper areas) at each wavelength, progressing to near-zero at brighter pixels (shallower areas).

4.1.2. Dual-channel model calibration

We optimized the dual-channel model (Eq. (4)) for three band combinations using quadratic regression. These included ratio-transforms based on reflectances from blue and green, blue and red, and green and red channels of WV-2 and Landsat 7 ETM+ sensors. Assessments of depth and band-ratio-derived quantity suggested moderately-strong to strong relations, with R^2 ranging from 0.67 to 0.81 (Fig. 5). As seen in Fig. 5, coupling of WV-2's blue and green wavelengths, as compared to ratios using the red band, appears to most accurately capture variations of X with respect to (D) depth ($R^2 = 0.81$), particularly over depths >5 m. The blue/red and green/red ratios lose sensitivity to depth changes at approximately $X > 2.0$ and 1.6 respectively. Therefore, inferring bathymetry using WV-2's red band, either directly or combined with the information in other spectral channels, will likely produce accurate results only for lake depths up to 5 m (Figs. 3 and 5). Similarly, OBRA analyses of ETM+ image spectra indicated optimal depth-retrieval based on blue and green measurements with an $R^2 = 0.84$ and standard deviation of 0.53 m ($d = 8.41\,X^2 + 1.4\,X - 0.017$).

4.2. Analysis of in situ depth-reflectance data

Given the availability of only 4-band WV-2 imagery over our primary study site (with three of the four bands being appropriate for lake depth analysis, namely blue, green, and red bands), we performed a theoretical simulation of WV-2 image spectra using in situ data over our second study site (Fig. 2), to determine optimal spectral channels for bathymetry for cases in which 8-band imagery is available. Using in situ measurements of depth and reflectance (Tedesco & Steiner, 2011a, 2011b), we simulated WV-2's signal by convolving the field spectra (n = 2226) with WV-2's spectral response function according to:

$$r_{nb} = \frac{\int_0^\infty r(\lambda)R(\lambda)d\lambda}{\int_0^\infty R(\lambda)d\lambda} \tag{5}$$

where r_{nb} is the narrowband reflectance, $r(\lambda)$ is the spectral reflectance, $R(\lambda)$ is the relative spectral response, and λ is wavelength (Pope et al., 2016). Convolved spectra and in situ depth measurements were then regressed according to the physically-based single-channel and dual-channel methods (see Eqs. (2) and (4)), results of which are summarized in Sections 4.2.1. and 4.2.2.

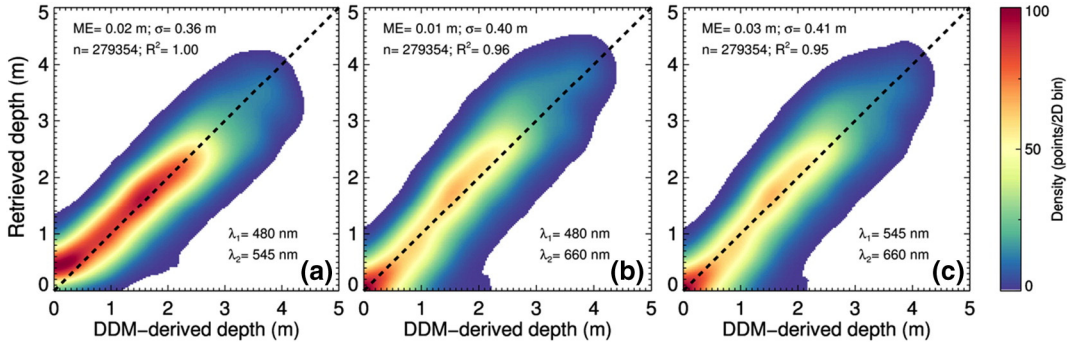

Fig. 8. 2D histograms (density plots) of spectrally-retrieved depths using dual-channel technique (Eq. (4)) vs. measured depths over the validation dataset (n = 279,354) a) blue & green ratio transform, b) blue & red ratio transform, and c) green & red ratio transform. (For interpretation of the references to color in this figure legend, the reader is referred to the web version of this article.)

4.2.1. Physically-based single-channel model

Our theoretical analysis based on simulated WV-2 signal in 6 spectral channels (WV-2 bands 1–6) indicate that WV-2's green, yellow, and red channels have the highest potential for retrieving lake depth (see Fig. 6 and Table 4). These bands show the strongest relationship between estimated and measured depth, with an RMSE < 1 m. As can be noted in Fig. 6, the red edge channel is unsuitable for lake depth analysis, due to the strong attenuation rate of radiation with depth in this part of the spectrum (705–745 nm). These findings reflect theoretical performances based on regressions of simulated WV-2 spectra against sonar-derived depths, which ranged from 1 to 4.6 m (Tedesco & Steiner, 2012). Green band data should be useful for depths up to 10–12 m, given the trend of our analysis. While coastal blue and blue channels might be able to map water depths of several 10s of meters, no supraglacial lakes on the GrIS or Antarctica are known to have depths of this magnitude.

We observed a large discrepancy between the parameters optimized using image spectra and those derived based on field spectra (see Tables 1 and 4). The simulated spectra and in situ depth measurements do not show the strong exponential relationship that image-derived data does (calibration dataset); the spread of the reflectance values is greater in the in situ data than in the image-derived data (see Figs. 3 and 6). It is possible that highly variable bottom albedo could have led to the spread of the in situ data. This variability would have been captured by the small footprint of the field measurements but smoothed out by the ~2 m pixels of WV-2. In addition, there are two orders of magnitude fewer in situ data points upon which to build a relationship. As a result, we do not recommend the coefficients reported in Table 4, especially those for coastal blue and blue bands, to be used for further studies. Nonetheless, conclusions in terms of optimal bands for bathymetry are expected to be robust.

4.2.2. Dual-channel model

We conducted OBRA analyses based on simulated WV-2 image spectra and in situ measured water depths, according to Eq. (4). The outcomes are displayed in Fig. 7 and Table 5. From this simulation excercise, it appears that combinations of WV-2 green & red, yellow & red, and green & yellow have the highest potential for retrieving lake depths. Other combinations also perform quite well, as measured by both R^2 and RMSE (see Table 5). These best-performing band combinations (see Fig. 7) are quite similar to those presented by Legleiter et al. (2014). Broadly, band combinations appear successful when in somewhat similar wavelengths in the visible portion of the spectrum, especially in the yellow and red wavelengths. As expected, the combination of near infrared bands, however, is very unsuccessful, given the strong absorption by water at those wavelengths. These results are based on sonar-derived lake depth measurements of up to 4.6 m (Tedesco & Steiner, 2011a, 2011b). Whether or not these results are applicable to depths beyond this range requires further investigation.

4.3. Validation of supraglacial lake bathymetry

The accuracy of spaceborne supraglacial bathymetry using our approach is influenced by many uncertainties including errors associated with classification, co-location, atmospheric correction, and DEM generation. In addition to these sources of uncertainty, a potential increase in lake depth over the observation period – i.e. length of time between multispectral and stereo image acquisition, which was shorter than 3 months for this study – could introduce further errors in measured post-drainage depths. This would result from lake-bottom ablation rates, which are observed to be up to 1.35× greater than the surrounding bare ice (Tedesco et al. 2012).

Based on the validation dataset (see Section 4.1), Table 6 summarizes the statistical performance of the different models in terms of four measures quantifying the difference between the spectrally-derived and the DDM-derived depths: mean error, RMSE, R^2, and percent volumetric error.

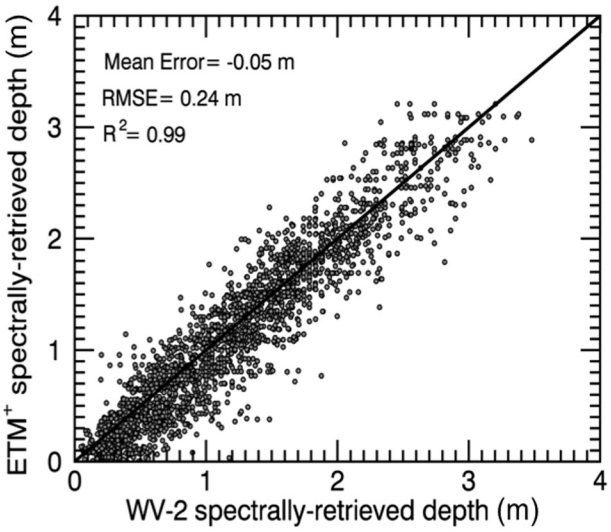

Fig. 9. Spectrally-retrieved depths based on WV-2's blue and green measurements vs. those obtained by Landsat 7's blue and green spectral reflectances (dual-channel method). As compared to WV-2, ETM+ results underestimated volume by 4%. (For interpretation of the references to color in this figure legend, the reader is referred to the web version of this article.)

4.3.1. Validation of depth-retrieval models

Assessments of depth estimates from physically-based and empirical single-channel models suggest strong statistical agreement with DDM-derived depths (average $R^2 = 0.9$). Overall, the depth estimates from the physically-based model (Eq. (2)) compare favorably to those obtained by the empirical model (Eq. (3)) (see Table 6). Using either technique, however, red channel measurements yield the least biased and most accurate depth estimates (mean error = 0.05 m, RMSE = 0.40 m), although it is important to note that the depths in the validation dataset were only up to ~4.5 m. Considering WV-2's red wavelength's reduced sensitivity to depth beyond 5 m, bathymetry over deeper lakes will be better resolved using WV-2's green band data (Fig. 3(b), Table 6).

Evaluation of results derived from the dual-channel model based on three band ratios (blue and green, blue and red, and green and red) pointed to its capability in retrieving depths with a high degree of accuracy (mean error < 1% of mean depth) and precision (RMSE = 0.4 m, ~<15% of mean depth). Comparison between estimated and measured lake volumes revealed an average (absolute) volumetric error of <1% (Table 6).

Overall, the performance of the dual-channel model, for all three band combinations, was better than for any single-channel model. This is likely due to lower sensitivity of the dual-channel method to substrate heterogeneity when compared to the single-channel technique. While the image-derived radiometric quantity in the dual-channel method tends to be only slightly sensitive to changes in substrate

Table 4
Parameters for and statistics on lake depth retrieval (Eq. (2)) based on simulated WV-2 reflectances (bands 1–6). Mean, standard deviation, and RMSE are all reported in meters.

WV-2 band	Spectral range (nm)	A_d	g (m^{-1})	R_∞	Mean	Std. dev.	RMSE
1 (Coastal blue)	400–450	0.30	0.03	0.045	3.72	12.57	12.60
2 (Blue)	450–510	0.29	0.04	0.000	3.12	3.60	3.49
3 (Green)	510–580	0.27	0.13	0.000	3.00	1.37	0.95
4 (Yellow)	585–625	0.21	0.52	0.004	2.98	1.06	0.36
5 (Red)	630–690	0.16	0.78	0.001	2.97	1.03	0.28
6 (Red edge)	705–745	0.03	2.98	0.000	2.88	0.86	0.41

Table 5
Parameters for and statistics on lake depth retrieval using quadratic optimal band ratio analysis of WV-2 band pairs as simulated from in situ spectra (Eq. (4)).

Band ratio	*a*	*b*	*c*	R^2	RMSE (m)
Green & red (3 & 5)	0.16	0.93	−0.29	0.97	0.16
Yellow & red (4 & 5)	1.06	1.57	−0.22	0.97	0.16
Green & yellow (3 & 4)	0.38	2.06	−0.35	0.97	0.17
Blue & red (2 & 5)	0.08	0.99	−0.44	0.96	0.19
Coastal blue & red (1 & 5)	0.07	0.96	−0.42	0.96	0.20
Blue & yellow (2 & 4)	0.06	2.00	−0.53	0.95	0.21
Coastal blue & yellow (1 & 4)	0.06	1.85	−0.48	0.94	0.23
Blue & green (2 & 3)	−5.41	11.67	−0.57	0.85	0.39

reflectance across bottom types (Legleiter et al., 2014), the spectral reflectance used in the single-channel methods has significant variability, especially going from bare ice to dark cryoconite holes (Tedesco & Steiner, 2011a, 2011b; Sneed and Hamilton, 2011).

Coupling of blue and green bands appears to most accurately capture the variations across a broader range of depths (Fig. 8), confirming conclusions from the calibration portion of this study. However, in the 0–1 m depth range, blue and green ratio exhibited the highest bias (0.1 m) when compared to the blue and red and green and red ratio transforms (Fig. 8). This bias may be partially due to path radiance residuals (remaining atmospheric effects). Our results indicate that over shallow water bodies (0–1 m), using WV-2's red band in the denominator of the dual-channel model (i.e. blue and red ratio, green and red ratio) will produce more accurate results than using the green band in the denominator. Conversely, over deeper lakes (depths > 5 m) using the green wavelength in the denominator (i.e. blue and green ratio) will yield more accurate depth and thus volume estimates, than using the red wavelength in the denominator. Lake depths ranging between 1–5 m are resolved similarly well using blue and green, blue and red, and green and red band ratios. These results are in line with findings from the analysis of field spectra by Legleiter et al. (2014).

Based on WV-2 multispectral measurements over our primary study area (Fig. 1) and depth-retrieval models, we found the maximum lake depth, area and volume to be 7 m, 3.48 km^2 and 0.08×10^{-2} km^3 respectively. To estimate the total amount of of meltwater in lakes, streams, and rivers captured by the WV-2 images (acquired on June 12, 2011), we applied our calibrated depth-retrieval models to areas of images where water pixels were present. Our analysis indicated that the total volume of meltwater stored in supraglacial lakes, streams, and rivers was $0.76 \pm 0.01 \times 10^{-2}$ km^3 (~65% of which was contained in twenty two lakes).

4.3.2. Comparison of WV-2 and Landsat 7 ETM + lake depth-retrievals

We also compared spectrally-retrieved depths from WV-2 imagery against those derived from the ETM+ scene of our primary study site (Fig. 1), using the validation datasets independently developed for these sensors. These comparisons suggested very strong statistical agreement with an average $R^2 = 0.98$ across various single- and dual-channel methods, an example of which is presented in Fig. 9. Consistent performance of WV-2 and ETM+ sensors is indicative of ETM+'s capability to accurately retrieve supraglacial water depths, despite offering lower spatial, spectral, and radiometric detail compared to the WV-2 sensor. Data loss resulting from Landsat 7's failed Scan Line Corrector (SLC) remains a limiting factor, because lakes are not imaged in their entirety further from the center line of the image. With higher radiometric resolution and better Signal-to-Noise ratio levels, the Operational Land Imager (OLI) on board the Landsat 8 satellite complements and improves upon Landsat 7 ETM^+ lake depth retrievals (Pope et al., 2016).

5. Conclusions

In this study, we perform an image-based retrieval of supraglacial lake depths using established models, completely independent from in situ data, and make recommendations on optimal spectral channels for bathymetry based on WV-2 and Landsat 7 ETM^+ imagery. To improve upon the limitations of using physical measurements of water depth to calibrate model parameters, we developed a methodology that eliminates the need for costly field or airborne bathymetric surveys. To calibrate the depth-retrieval parameters of these models, we used lake reflectances recorded by the WV-2 and Landsat 7 ETM+ sensors for filled lakes and coupled them with co-located elevation measurements from a high-resolution post-drainage WV-2 DEM. Our analysis suggests that, For both the WV-2 and the L7 ETM^+ sensor, the optimal depth-retrieval method depends on the maximum lake depth and its distribution. Our analysis of 4-band WV-2 Images showed that for shallow lake areas ($d < 1$ m), the dual-channel model based on the green & red band ratio yields the most accurate results. All dual-channel models perform equally well for lake depths between 1 and 5 m. For deeper lakes ($d > 5$ m), the blue & green band ratio resolves depths more accurately than other band combinations. Similarly, single-channel models based on red band data are only accurate for lake depths up to 5 m. Green band data is best for deeper lakes (>5 m). Our theoretical assessment of 8-band WV-2 imagery indicated that with single-channel models, the green, yellow, and red channels are most suitable for accurate bathymetry. For dual-channel models, band ratios based on WV-2's green & red, yellow & red, green & yellow spectral channels have the highest potential for retrieving supraglacial lake depths. These results are consistent with the findings based on image-data analysis.

Our assessments of single-channel and dual-channel bathymetry models indicate that, overall, dual-channel models can resolve depths more accurately than single-channel models. Depths retrieved with the dual-channel method showed high accuracy (mean error < 1% of mean depth) and precision (RMSE < 15% of mean depth) across various band ratios. Moreover, the average error in lake volume estimation across a ~1250 km^2 area was <1%, which is unprecedented for spaceborne supraglacial bathymetry.

Remote sensing continues to provide valuable tools for monitoring the areal extent, depths, and thus volumes of supraglacial lakes, the studies of which are important for understanding ice dynamics and thermodynamic processes. We have presented a new methodology to characterize and validate meltwater storage volumes purely based on

Table 6
Statistics on lake depth retrieval using single-channel (Eq. (2) and Eq. (3)) and dual-channel (Eq. (4)) methods based on WV-2 measurements (validation dataset, n = 279,354).

λ_1^c (nm)	λ_2^c (nm)	Mean error (m)		RMSE (m)		OP R^2		Volume error (%)	
		Single-channel model							
		Physical	Empirical	Physical	Empirical	Physical	Empirical	Physical	Empirical
480	–	0.17	0.11	0.54	0.64	0.83	0.80	11.46	13.45
545	–	0.10	0.06	0.42	0.49	0.92	0.91	5.68	7.03
660	–	0.06	0.05	0.35	0.45	0.95	0.91	1.12	4.27
		Dual-channel model							
480	545	0.02		0.36		0.99		0.15	
545	660	0.01		0.40		0.96		−0.31	
660	660	0.03		0.41		0.95		1.62	

remotely-sensed data. This method allows for calibration of lake depths over both small and large lakes in an extended study area, leading to an improved representation of supraglacial lake population. For site-specific studies, calibration of models based on the approach in this paper (image-based retrieval of model parameters) is strongly preferred to application of models based on theoretical/estimated values of lake/water optical properties. Our approach does not rely on images covering both the ice sheet and the adjacent ice-free ocean regions to retrieve R_∞(reflectance of optically-deep water), which allows using ice sheet interior imagery from narrow- to moderately-wide-swath instruments with medium-to-high spatial resolution (WV-2, ASTER, and Landsat). Additionally, the method's success in capturing lake margin depths with high accuracy offers potential to characterize transient meltwater flow through shallow supraglacial streams and rivers, which has important implications for understanding ice sheet hydrology (Smith et al., 2015). This study demonstrates successful application of depth-retrieval models over a relatively large area; however, more data are required to build models for ice sheet-wide estimation of supraglacial water depths. Given the rapid expansion in the availability of imagery from high-resolution and stereo sensors for scientific use, this methodology represents a significant opportunity to expand our capability of supraglacial lake volume estimates across Greenland and other glaciated regions.

Acknowledgments

This work was supported by the National Aeronautics and Space Administration (NASA) [grant number NNX10AR76G]. The Polar Geospatial Center at the University of Minnesota, supported by the U.S. National Science Foundation (NSF) [grant ANT-1043681], provided the WorldView imagery. A. Pope and T. Scambos were supported by U.S. Geological Survey contract G12PC00066. We thank Dr. Carl J. Legleiter from the University of Wyoming for his support and helpful comments.

References

Aguilar, M. A., del Mar Saldana, M., & Aguilar, F. J. (2014). "Generation and quality assessment of stereo-extracted DSM from GeoEye-1 and WorldView-2 imagery. *Geoscience and Remote Sensing, IEEE Transactions on*. http://dx.doi.org/10.1109/TGRS.2013.2249521.

Arnold, N. S., Banwell, A. F., & Willis, I. C. (2014). High-resolution modelling of the seasonal evolution of surface water storage on the Greenland Ice Sheet. *The Cryosphere*, *8*(4), 1149–1160. http://dx.doi.org/10.5194/tc-8-1149-2014.

Banwell, A. F., Caballero, M., Arnold, N. S., Glasser, N. F., Cathles, L. M., & MacAyeal, D. R. (2014). Supraglacial lakes on the Larsen B ice shelf, Antarctica, and at Paakitsoq, West Greenland: a comparative study. *Annals of Glaciology*, *55*(66), 1–8. http://dx.doi.org/10.3189/2014AoG66A049.

Bartholomew, I. D., Nienow, P., Sole, A., Mair, D., Cowton, T., King, M. A., & Palmer, S. (2011). "Seasonal variations in Greenland Ice Sheet motion: inland extent and behaviour at higher elevations. *Earth and Planetary Science Letters*, *307*(3–4), 271–278 (Elsevier B.V. doi:10.1016/j.epsl.2011.04.014).

Bartholomew, I., Nienow, P., Sole, A., Mair, D., Cowton, T., & King, M. A. (2012). Short-term variability in Greenland Ice Sheet motion forced by time-varying meltwater drainage: Implications for the relationship between subglacial drainage system behavior and ice velocity. *Journal of Geophysical Research*, *117*(F3), F03002. http://dx.doi.org/10.1029/2011JF002220.

Berke, A. (2006). MODTRAN5: 2006 update. *International society for optics and photonics*.

Box, J. E., & Ski, K. (2007). Remote sounding of Greenland supraglacial melt lakes: implications for subglacial hydraulics. *Journal of Glaciology*, *53*(181), 257–265. http://dx.doi.org/10.3189/172756507782202883.

Catania, G., Neumann, T., & Price, S. (2008). Characterizing englacial drainage in the ablation zone of the Greenland Ice Sheet. *Journal of Glaciology*, *54*, 567–578.

Das, S. B., Joughin, I., Behn, M. D., Howat, I. M., King, M. A., Lizarralde, D., & Bhatia, M. P. (2008). "Fracture propagation to the base of the Greenland Ice Sheet during supraglacial lake drainage. *Science*, *320 (5877)*, 778–781. http://dx.doi.org/10.1126/science.1153360 (New York, N.Y.).

DigitalGlobe (2014). Geolocation Accuracy of WorldView Products. http://global.digitalglobe.com/sites/default/files/WorldView_Geolocation_Accuracy.pdf

Fitzpatrick, A. A. W., Hubbard, A. L., Box, J. E., Quincey, D. J., van As, D., Mikkelsen, A. P. B., ... Jones, G. A. (2014). A decade (2002–2012) of supraglacial lake volume estimates across Russell Glacier, West Greenland. *The Cryosphere*, *8*(1), 107–121. http://dx.doi.org/10.5194/tc-8-107-2014.

Flood, N. (2014). "Continuity of reflectance data between Landsat-7 ETM + and Landsat-8 OLI, for both top-of-atmosphere and surface reflectance: A study in the Australian landscape. *Remote Sensing*. http://dx.doi.org/10.3390/rs6097952.

Georgiou, S., Shepherd, A., McMillan, M., & Nienow, P. (2009). Seasonal evolution of supraglacial lake volume from ASTER imagery. *Annals of Glaciology*, *50*(52), 95–100. http://dx.doi.org/10.3189/172756409789624328.

Hoffman, M. J., Catania, G. A., Neumann, T. A., Andrews, L. C., & Rumrill, J. A. (2011). Links between acceleration, melting, and supraglacial lake drainage of the western Greenland Ice Sheet. *Journal of Geophysical Research*, *116*(F4), F04035. http://dx.doi.org/10.1029/2010JF001934.

Legleiter, C. J., Roberts, D. A., & Lawrence, R. L. (2009). Spectrally based remote sensing of river bathymetry. *Earth Surface Processes and Landforms*, *34*(8), 1039–1059.

Legleiter, C. J., Tedesco, M., Smith, L. C., Behar, A. E., & Overstreet, B. T. (2014). Mapping the bathymetry of supraglacial lakes and streams on the Greenland Ice Sheet using field measurements and high-resolution satellite images. *The Cryosphere*, *8*(1), 215–228. http://dx.doi.org/10.5194/tc-8-215-2014.

Markwardt, C. (2009). Non-linear least squares fitting in IDL with MPFIT. In D. Bohlender, D. Dowler, & P. Durand (Eds.), *Stronomical data analysis software and systems XVIII* (pp. 251–254) (Quebec, Canada).

McMillan, M., Nienow, P., Shepherd, A., Benham, T., & Sole, A. (2007a). Seasonal evolution of supra-Glacial Lakes on the Greenland Ice Sheet. *Earth and Planetary Science Letters*, *262*(3–4), 484–492. http://dx.doi.org/10.1016/j.epsl.2007.08.002.

Menzel, W. P., et al. (2002). *MODIS atmospheric profile retrieval algorithm theoretical basis document, version 6, reference number: ATBD-MOD-07*.

Mitchell, G. (2010). "PhotoSat WorldView-2 Stereo Satellite DEM Comparison to a LiDAR DEM over the Garlock Fault in Southeast California. https://www.digitalglobe.com/sites/default/files/PhotoSat (WV-2 Stereo Satellite DEM Comparison_0.pdf)

Padwick, C. (2010). WorldView-2 pan-sharpening. *American society for photogrammetry and remote sensing (asprs) annual conference* (San Diego, CA).

Palmer, S., Shepherd, A., Nienow, P., & Joughin, I. (2011). "Seasonal speedup of the Greenland Ice Sheet linked to routing of surface water. *Earth and Planetary Science Letters*, *302*(3–4), 423–428 (Elsevier B.V. doi:10.1016/j.epsl.2010.12.037).

Phillips, T., Rajaram, H., Colgan, W., Steffen, K., & Abdalati, W. (2013). Evaluation of cryo-hydrologic warming as an explanation for increased ice velocities in the wet snow zone, Sermeq Avannarleq, West Greenland. *Journal of Geophysical Research - Earth Surface*, *118*(3), 1241–1256. http://dx.doi.org/10.1002/jgrf.20079.

Philpot, W. D. (1989). Bathymetric mapping with passive multispectral imagery. *Applied Optics*, *28*(8), 1569–1578.

Pope, A., Scambos, T. A., Moussavi, M., Tedesco, M., Willis, M., Shean, D., & Grigsby, S. (2016). "Estimating supraglacial lake depth in west Greenland using landsat 8 and comparison with other multispectral methods. *The Cryosphere*, *10*(1), 15–27 (Copernicus Publications doi:10.5194/tc-10-15-2016).

Pope, R. M., & Fry, E. S. (1997). "Absorption spectrum (380–700 nm)pure water. II. Integrating cavity measurements. *Applied Optics*.

Rignot, E., Velicogna, I., van den Broeke, M. R., Monaghan, A., & Lenaerts, J. T. M. (2011). "Acceleration of the contribution of the greenland and antarctic ice sheets to sea level rise. *Geophysical Research Letters*, *38*(5) (n/a–n/a. doi:10.1029/2011GL046583).

Schläpfer, D., & Nieke, J. (2005). "Operational simulation of at sensor radiance sensitivity using the MODO/MODTRAN4 environment. *Proceedings EARSeL fourth workshop on imaging spectroscopy* (Warsaw. Poland).

Schrama, J O]–>E. J. O., & Wouters, B. (2011). Revisiting Greenland Ice Sheet mass loss observed by GRACE. *Journal of Geophysical Research: Solid Earth*, *116*(B2) (n/a–n/a. doi:10.1029/2009JB006847).

Selmes, N., Murray, T., & James, T. D. (2011). "Fast draining lakes on the Greenland Ice Sheet. *Geophysical Research Letters*, *38*(15) (n/a–n/a. doi:10.1029/2011GL047872).

Selmes, N., Murray, T., & James, T. D. (2013). Characterizing supraglacial lake drainage and freezing on the Greenland Ice Sheet. *The Cryosphere Discussions*, *7*(1), 475–505. http://dx.doi.org/10.5194/tcd-7-475-2013.

Shean, D. E., Alexandrov, O., Moratto, Z. M., Smith, B. E., Joughin, I. R., Porter, C. C., & Morin, P. J. (2016). *An automated, open-source pipeline for mass production of digital elevation models (DEMs) from very-high-resolution commercial stereo satellite imagery.*

Shepherd, A., Ivins, E. R., Geruo, A., Barletta, V. R., Bentley, M. J., Bettadpur, S., Briggs, K. H., et al. (2012). "A reconciled estimate of ice-sheet mass balance. *Science*, *338 (6111)*, 1183–1189. http://dx.doi.org/10.1126/science.1228102 (New York, N.Y.).

Smith, L. C., Chu, V. W., Yang, K., Gleason, C. J., Pitcher, L. H., Rennermalm, A. K., Legleiter, C. J., et al. (2015). Efficient meltwater drainage through supraglacial streams and rivers on the Southwest Greenland Ice Sheet. *Proceedings of the National Academy of Sciences*, *112*(4), 1001–1006. http://dx.doi.org/10.1073/pnas.1413024112.

Smith, R. C., & Baker, K. S. (1981). "Optical properties of the clearest natural waters (200–800 Nm). *Applied Optics*, *20*(2), 177–184 OSA. (doi:10.1364/AO.20.000177).

Sneed, W. A., & Hamilton, G. S. (2007). Evolution of melt pond volume on the surface of the Greenland Ice Sheet. *Geophysical Research Letters*, *34*(3), L03501. http://dx.doi.org/10.1029/2006GL028697.

Sneed, W. A., & Hamilton, G. S. (2011). Validation of a method for determining the depth of glacial melt ponds using satellite imagery. *Annals of Glaciology*, *52*(59), 15–22. http://dx.doi.org/10.3189/172756411799096240.

Stevens, L. A., Behn, M. D., McGuire, J. J., Das, S. B., Joughin, I., Herring, T., ... King, M. A. (2015). "Greenland supraglacial lake drainages triggered by hydrologically induced basal slip. *Nature*, *522 (7554)*, 73–76 Nature Publishing Group, a division of Macmillan Publishers Limited. All Rights Reserved. (10.1038/nature14480).

Swinehart, D. F. (1962). The Beer–Lambert law. *Journal of Chemical Education*, *39*(7), 333. http://dx.doi.org/10.1021/ed039p333.

Tedesco, M., Lüthje, M., Steffen, K., Steiner, N., Fettweis, X., Willis, I., ... Banwell, A. (2012). Measurement and modeling of ablation of the bottom of supraglacial lakes in western Greenland. *Geophysical Research Letters*, *39*(2). http://dx.doi.org/10.1029/2011GL049882.

Tedesco, M., & Steiner, N. (2011a). "The cryosphere in-situ multispectral and bathymetric measurements over a supraglacial lake in western Greenland using a remotely controlled watercraft" *1*, 445–452. http://dx.doi.org/10.5194/tc-5-445-2011.

Tedesco, M., & Steiner, N. (2011b). In-situ multispectral and bathymetric measurements over a supraglacial lake in western Greenland using a remotely controlled watercraft. *The Cryosphere*, *5*(2), 445–452. http://dx.doi.org/10.5194/tc-5-445-2011.

Tedesco, M., Willis, I. C., Hoffman, M. J., Banwell, A. F., Alexander, P., & Arnold, N. S. (2013). Ice dynamic response to two modes of surface lake drainage on the Greenland Ice Sheet. *Environmental Research Letters*, *8*(3), 034007. http://dx.doi.org/10.1088/1748-9326/8/3/034007.

van den Broeke, M., Bamber, J., Ettema, J., Rignot, E., Schrama, E., van de Berg, W. J., ... Wouters, B. (2009). Partitioning recent Greenland mass loss. *Science*, *326*(5955), 984–986. http://dx.doi.org/10.1126/science.1178176.

Willis, M. J., Herried, B. G., Bevis, M. G., & Bell, R. E. (2015). Recharge of a subglacial lake by surface meltwater in Northeast Greenland. *Nature*, *518*(7538), 223–227. http://dx.doi.org/10.1038/nature14116.

Wouters, B., Chambers, D., & Schrama, J O]–>E. J. O. (2008). "Grace observes small-scale mass loss in Greenland. *Geophysical Research Letters*, *35*(20) (n/a–n/a. doi:10.1029/2008GL034816).

Yang, K., & Smith, L. C. (2013). Supraglacial streams on the Greenland Ice Sheet delineated from combined spectral–shape information in high-resolution satellite imagery. *IEEE Geoscience and Remote Sensing Letters*, *10*(4), 801–805. http://dx.doi.org/10.1109/LGRS.2012.2224316.

Zwally, H. J., Abdalati, W., Herring, T., Larson, K., Saba, J., & Steffen, K. (2002). "Surface melt-induced acceleration of Greenland ice-sheet flow. *Science*, *297 (5579)*, 218–222. http://dx.doi.org/10.1126/science.1072708 (New York, N.Y.).